

Fatigue crack evolution and effect analysis of Ag sintering die-attachment in SiC power devices under power cycling based on phase-field simulation

Yutai Su^a, Guicui Fu^{a,*}, Changqing Liu^b, Canyu Liu^b, Xu Long^c

^a School of Reliability and System Engineering, Beihang University, Beijing, PR China

^b Wolfson School of Mechanical, Electrical and Manufacturing Engineering, Loughborough University, Leicestershire, United Kingdom

^c School of Mechanics, Civil Engineering and Architecture, Northwestern Polytechnical University, Xi'an, PR China



ARTICLE INFO

Keywords:

Phase-field simulation
Fatigue crack evolution
Ag sintering die-attachment
SiC power devices

ABSTRACT

Sintering Ag materials is a promising candidate for the die-attachments in SiC power devices due to its high melting point and low thermal resistance. However, CTE mismatch between the SiC chips and the substrates causes cracks to develop in the sintered interconnection structures. Power cycling conditions lead to periodic loadings on the Ag sintering die-attachment. The incremental accumulation of plastic strain energy, combined with periodic fluctuations of elastic strain energy, results in the fatigue crack evolutions of the sintered structures. Further, the crack evolutions considerably degrade the thermal and mechanical properties of the interconnect structure, and critically affects the integrity of the heat transfer network and the mechanical structure of the power devices. In this paper, the fatigue crack evolution of Ag sintering die-attachment in the SiC power devices is simulated based on the phase-field models. Moreover, the thermal performance degradations and stress distributions of die-attachment under power cycling are analysed. A methodology based on finite element modelling and phase-field simulation is proposed, realised by Abaqus and its subroutines. The fatigue crack in the Ag sintering die-attachment initiates from the chip-side corner point, then propagates to the chip-side centre point until the formation of a penetrative crack, which achieves a good match with experimental results. Moreover, along with the crack propagation, the thermal distributions in the chip and the stress distributions of the sintering layer are obtained to analyse the degradations of thermal and mechanical performances of Ag sintering die-attachment in SiC power devices.

1. Introduction

Silicon carbide (SiC) power devices, with a wide bandgap, a high critical electric field and a high thermal conductivity, have a broad application prospect in the field of power electronics [1]. Due to the harsh working environment and high-power loads, the reliability issues of the die-attachment in SiC power devices, such as fatigue crack propagation, thermal resistance increase and electrical deterioration or even failure, have been attracted considerable attention.

SiC power device is a multi-layer structure composed of various materials with different coefficients of thermal expansion (CTE). Due to the CTE mismatch, thermal cycling or power cycling causes cyclic stress loads in the die-attachments where fatigue cracks appear [2,3]. Moreover, fatigue crack propagation has an evident influence on the thermal conductivity and stress field distribution of the die-attachment layers [4].

Ag sintering die-attachments can be configured as thermo-elasto-plastic solids [5,6]. Fracture Phase-field method is used to simulate the crack evolutions in the solids. Miehe et al. proposed a phase-field model for brittle fractures to analyse the crack propagations and obtain the mechanical behaviours [7]. Then, Molnár et al. implemented this phase-field model by Abaqus and its subroutines [8]. Further, Dittmann et al. established a thermo-elasto-plastic phase-field model to simulate the ductile fracture [9]. Meanwhile, extensive experimental and numerical studies have been conducted that could support the phase-field models for the Ag sintering attachments in the SiC power devices [10,11].

In this study, we have investigated in the fatigue crack evolution of Ag sintering die-attachment in SiC power devices and analysed its effects on the thermal performance and stress distributions of the die-attachments under power cycling. A methodology based on finite element (FE) modelling and phase-field simulation is proposed to

* Corresponding author.

E-mail address: fuguicui@buaa.edu.cn (G. Fu).

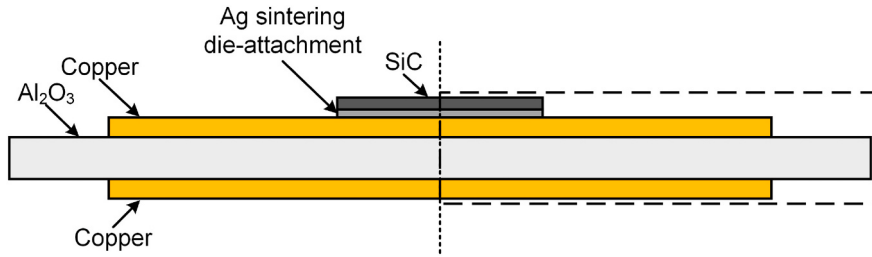


Fig. 1. 2D structure diagram of the SiC power devices.

Table 1
The sizes of each layer in the SiC power device.

Material layer	Length (mm)	Thickness (μm)
SiC chip	3.1	180
Ag sintering die-attachment	3.1	120
Top copper layer	10.0	300
Al_2O_3 layer	13.0	630
Bottom copper layer	10.0	300

describe the crack initiation and propagation in the die-attachment, which utilises the Abaqus and its subroutines. Moreover, the simulation results are reasonable and accord with the experiments well.

2. Finite element modelling

A typical SiC power device, to perform the fracture phase-field simulations and analyse the effects of the crack evolutions, is proposed. The device is stacked in sequence by SiC chip, Ag sintering die-attachment and alumina direct bonded copper (DBC) substrate, as shown in Fig. 1. The sizes of each layer in this 2D model are detailed in Table 1.

Then, a typical power cycling load is applied to the top central area of the chip. Considering the mission profile of the SiC power devices, the cyclic period time is 2 h, in which 1 h is power off and the other 1 h is power on with an amplitude of $5.78 \times 10^9 \text{ W/m}^3$, as shown in Fig. 2. The power cycling continues until the die-attachment completely detaches from the chip due to fatigue cracking.

Assume that the SiC chip, copper layers and Al_2O_3 ceramic layer are thermo-elastic solids. Meanwhile, suppose that the sintered Ag is thermo-elasto-plastic solids, and the mechanical behaviours of sintered Ag follow the bilinear elasto-plastic constitutive model. The reference temperature is 293.15 K. Thereby, thermo-mechanical properties of the materials in the device are listed in Table 2, which could support the material definitions of the FE model in Abaqus.

Further, the thermal and mechanical boundary conditions are defined, shown in Fig. 3. For the thermal boundary conditions, the

bottom of this model is a heat sink surface with a constant room temperature. A selected top area with a red line in the model is a heat flux, and the profile of this heat flux is shown in Fig. 2. The other external boundaries of the model are set as thermal insulations. To set the mechanical boundary conditions, the bottom is fixed in the Y direction, also regarded as a roller constrain.

Meanwhile, this model is strategically meshed as Fig. 3. The region of the chip is meshed as 6200 quadrilateral elements, the region of the die-attachment is meshed as 14,880 quadrilateral elements, and the region of DBC is meshed as 10,566 quadrilateral elements and 16,478 triangular elements.

3. Fracture phase-field model

Fracture phase-field model is proposed to describe the crack evolution in the sintered Ag die-attachment. Assume a regularised sharp crack follows an exponential fracture phase-field function [7], given by

$$d(x) = e^{-\frac{|x|}{l_c}}, \quad (1)$$

where l_c is the length scale that interprets the width of the sharp crack. A one-dimensional diffusive crack at $x = 0$ with the length scale l_c is shown in Fig. 4.

Based on this phase-field model, the fracture surface energy can be approximately expressed as

$$\int_{\Gamma} g_c d\Gamma = \int_{\Omega} \frac{g_c}{2l_c} (d^2 + l_c^2 |\nabla d|^2) d\Omega, \quad (2)$$

where g_c is the fracture surface energy per unit. Further, the phase-field fracture energy density could be given by

$$\psi^d = \frac{g_c}{2l_c} (l_c^2 \nabla d \cdot \nabla d + d^2) \quad (3)$$

Based on the thermo-mechanical coupling process, the multi-physical field interaction mechanism of the die-attachment fracturing could be defined as Fig. 5. This mechanism involves three fundamental processes, including thermal process, mechanical process and fracturing

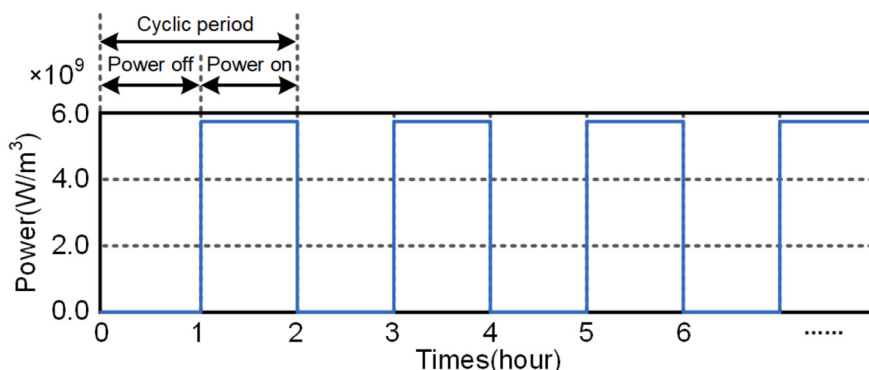


Fig. 2. Power cycling profile of the SiC power device.

Table 2
Materials properties in the FE model [10,11].

Material	Properties	Value	Unit
SiC	CTE	3.4	$10^{-6}/K$
	Young's modulus	501.0	GPa
	Poisson's ratio	0.45	1
	Thermal conductivity	370.0	W/(m·K)
	Thermal capacity	690.0	J/(kg·K)
Sintered Ag		14.2 (100.15 K)	
	CTE	18.9 (298.15 K)	$10^{-6}/K$
		20.6 (423.15 K)	
		14.2 (233.15 K)	
	Young's modulus	10.1 (298.15 K)	GPa
		8.0 (423.15 K)	
		0.34 (233.15 K)	
	Poisson's ratio	0.34 (298.15 K)	1
		0.20 (423.15 K)	
		35.4 (233.15 K)	
Cu	Yield strength	21.8 (298.15 K)	MPa
		16.1 (423.15 K)	
		0.36 (233.15 K)	
	Hardening modulus	4.32 (298.15 K)	GPa
		2.11 (423.15 K)	
Al_2O_3	Thermal conductivity	50.0	W/(m·K)
	Thermal capacity	170.0	J/(kg·K)
	CTE	17.0	$10^{-6}/K$
	Young's modulus	110.0	GPa
	Poisson's ratio	0.35	1

process. Heat transfer and thermal expansion could induce the non-uniform thermal, stress and strain distributions. During the cyclic loading, the plastic strain energy dissipations with the periodic fluctuations of elastic strain energy arise, leading to the crack evolution in the fracture process. The crack evolution in die-attachment could affect both

thermal and mechanical processes due to the increase of the failure elements in the models.

Considering this fracture mechanism, the total energy functionals could be given by:

$$\psi = \psi^e(\epsilon^e, \theta, d) + \psi^p(\gamma^p, \theta, d) + \psi^d(d), \quad (4)$$

where ψ^e is the elastic energy density related to the crack value d , temperature θ , and the elastic strain tensor ϵ^e . ψ^p is the plastic energy density related to the crack d , temperature θ , and the cumulative plastic strain γ^p . ψ^d is the phase-field fracture energy density, as shown in Eq. (3). The fracture parameters of sintered Ag are listed in Table 3.

Refer to our previous work [12], the systems of the governing equations for this thermo-mechanical coupled problem could be built, and the spatial and temporal discretization is performed. Then, the two-

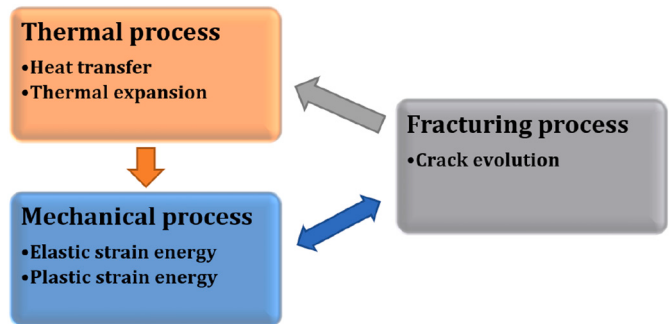


Fig. 5. The multi-physical process of the die-attachment fracturing.

Table 3
Fracture parameters of sintered Ag.

Parameter	Value	Unit
Length scale parameter (l_c)	0.025	-
Fracture surface energy (g_c)	0.000003	-

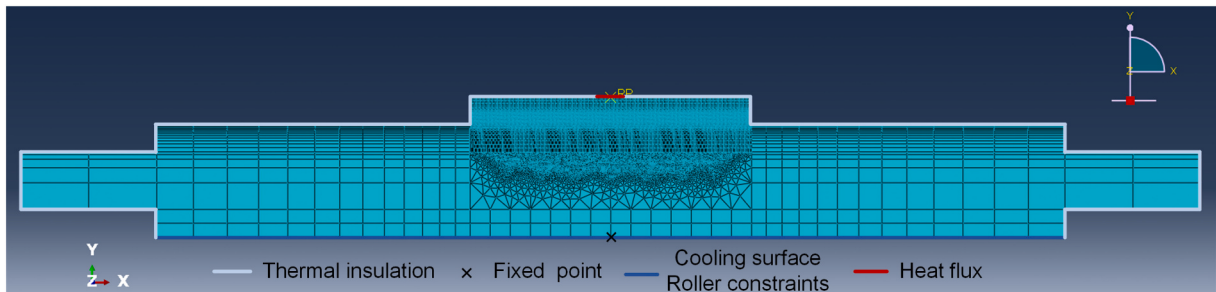


Fig. 3. Boundary conditions and mesh generations of the FE model.

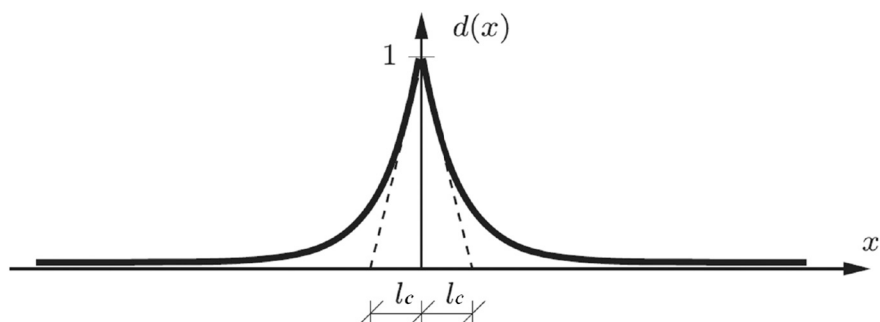


Fig. 4. Diffusive fracture phase-field models (crack at $x = 0$ modelled with the length scale l_c) [7].

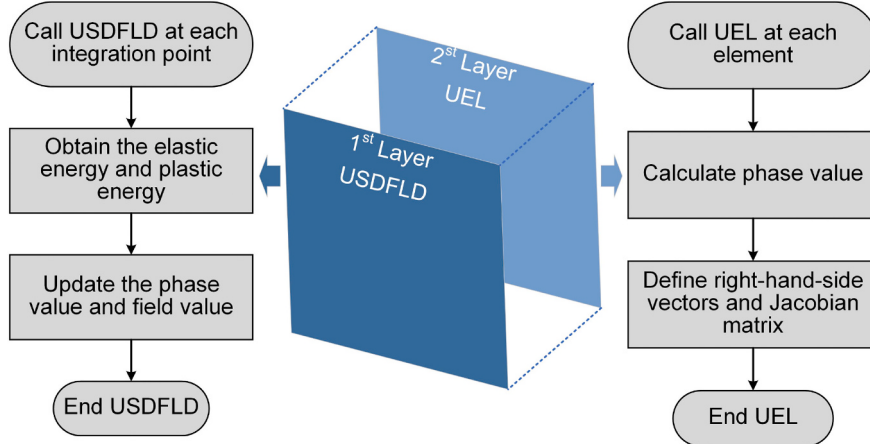


Fig. 6. The two-layer structure of the phase-field simulation.

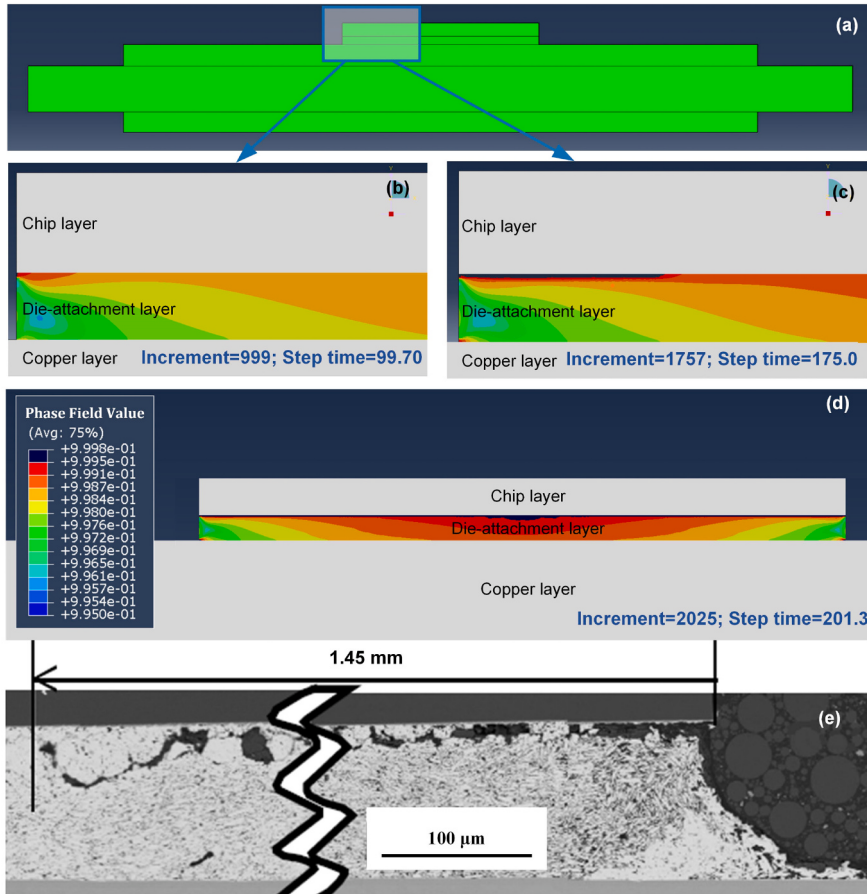


Fig. 7. Phase-field simulation results of fatigue crack evolution [11].

layer structure of this fracture phase-field simulation is constructed by Abaqus and its subroutine as Fig. 6. The first layer is implemented by the subroutine USDFLD (user defined field), obtaining the elastic and plastic strain energy. The second layer is realised by the subroutine UEL (user defined element).

Here, more 14,880 elements are written in the input file to calculate the phase-field value of each element in the die-attachment. And the subroutines are written by the FORTRAN code. Utilizing the input file and the subroutine files, the fracture phase-field simulation of the die-attachment in the SiC power device is performed by the Abaqus software.

4. Results and discussion

Combined with the FE and fracture phase-field models, the fatigue crack evolution in the die-attachment of the SiC power device could be simulated. Based on the fatigue crack evolution, thermal performance degradations and stress distribution variations are further analysed and discussed by the proposed methods.

4.1. Fatigue crack evolution analysis for die-attachment

The fatigue crack propagation is symmetric to the middle plane of

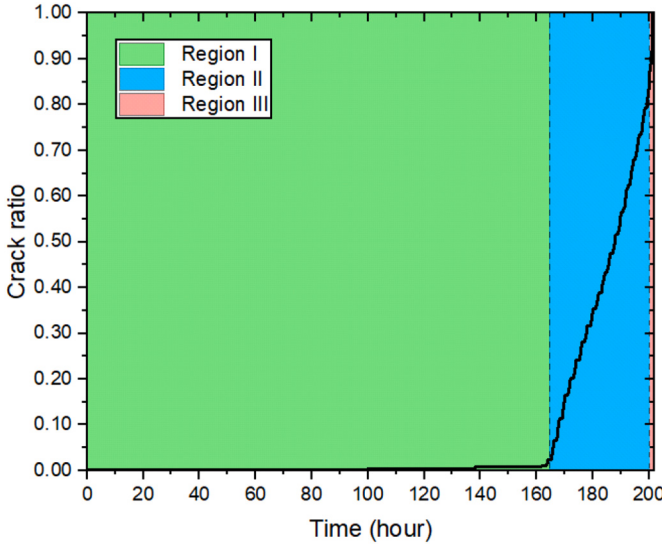


Fig. 8. The growth of crack ratio over time by simulations.

the FE model so that the left region of the die-attachment is zoomed in as Fig. 7 (a). The phase-field values of the die-attachment are calculated. Assume the threshold of phase-field value for fracture is 0.9995, the crack morphologies with three different increments could be shown in Fig. 7 (b) (c) (d). The fatigue cracks initiate from the chip-side corners and propagate along with the interface between the die-attachment and the chip. Finally, the fatigue crack horizontally penetrates the interconnect structure of this device, leading to the failure of this die-attachment. The morphologies and evolution routes of the fatigue crack are in good agreement with experimental results [11] as Fig. 7 (e). Remarkably, Fig. 7 (b) shows the initial fracture element appears in the 50th cycle when the first element break. And Fig. 7 (d) presents the penetrating fatigue crack in the 101st cycle leading to the complete fracture in the die-attachment. Compared with these two cycle times, the occurrence of the first fracture element cost 49.5% lifetime, nearly half of the total lifetime.

The crack ratio, fracture length divided by die-attachment length, with increasing time is obtained by counting the fracture elements at each time increment, as shown in Fig. 8. The figure could be clearly distinguished into three regions. Region I is the crack initiation phase, which ranges from 0 to 166 h (from 0 to 83 cycles), with a crack ratio of only 1%. Region II is the crack propagation phase, where the crack ratio increases with a constant crack increase rate, 0.026 per hour. This region starts from 166 to 200 h with an increasing 90% of the crack ratio.

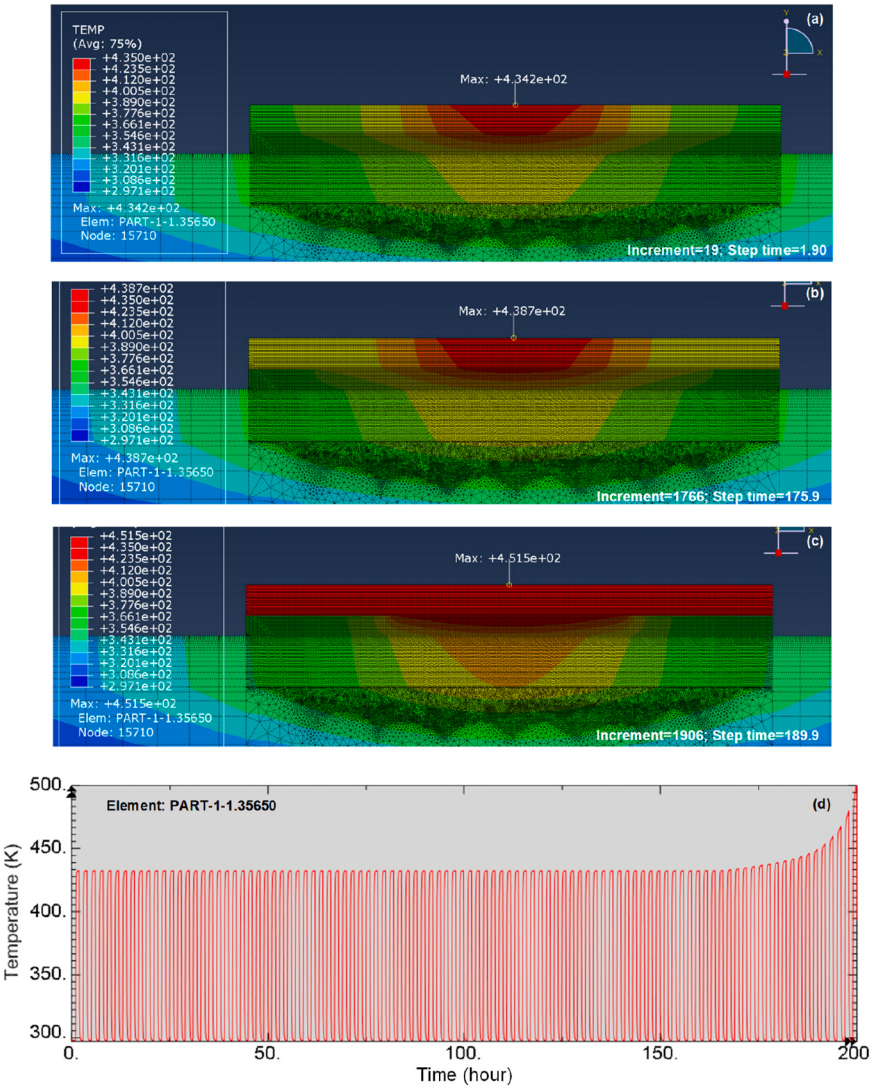


Fig. 9. Thermal performance degradation caused by crack evolution.

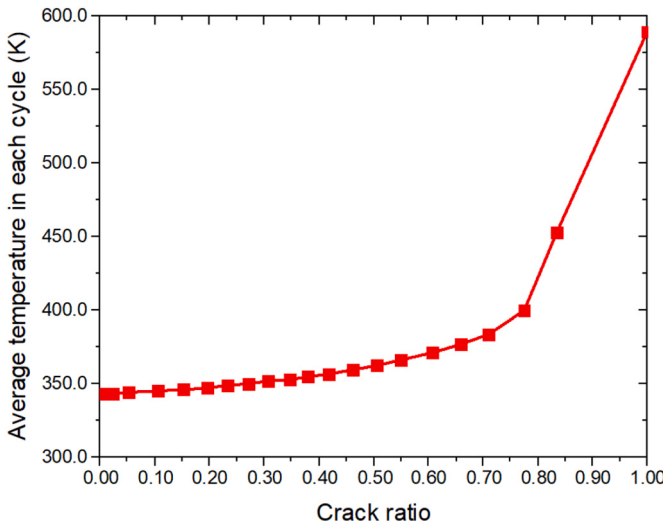


Fig. 10. The average temperature of the top surface on the chip in each power cycle with different crack ratios.

Region III occurs in the last cycle from 200 to 202 h. The Ag sintering die-attachment, with the only remaining 10%, fractured instantly in the last cycle. Finally, the horizontal penetration crack is formed, and the interconnect structure between the chip and the substrate has lost its mechanical support and thermal and electrical conductivity.

4.2. Thermal performance degradation analysis

Fatigue cracks in the die-attachment affect the thermal conductivity of the interconnect structures in the power device, resulting in failures to transfer heat away from the chip and temperature increases in the chip. The thermal distributions of three different time increments are selected at the highest temperature status in the respective power cycles, shown in Fig. 9 (a) (b) (c). Fig. 9 (a) shows the initial maximum temperature in the chip under the power cycle is 434.2 K. The maximum temperature in the chip increases along with the crack propagation due to the reduced heat transfer path. When the fatigue life consumption reaches 94% (95 cycles), the maximum temperature in the chip rises up to 451.5 K. Compared with Fig. 9 (b) and (c), the heat transferable region is significantly reduced in the die-attachment, and the thermal distributions below the chip are concentrated in an inverted triangular shape. Additionally, the temperature curve of element 35,650, the top centre point on the SiC chip, is presented in Fig. 9 (d). Notably, the thermal conductivity of the sintered Ag material degrades slowly with increasing time.

Further, the average temperature on the top surface of the chip in each power cycle with the different crack ratio is shown in Fig. 10. Despite the existence of a large crack ratio, the effect on the thermal

performance of the sintered Ag die-attachment is not significant. As the crack ratio rises to 0.71, the average temperature only increases 41.16 K. However, a considerable temperature rise appears prior to a complete fracture.

4.3. Stress distributions in the die-attachment

Fig. 11 shows the stress distributions in the die-attachment. The initial maximum von Mises stress is about 28 MPa at the chip-side corners. Then, the concentrated stress points follow with the crack tip from the corner to the centre. Moreover, the maximum effective stress reaches 45.08 MPa before failure.

Five element points are chosen from corner to centre, and the stress-time curves are obtained as shown in Fig. 12. The maximum effective stress of corner element 29,141 reduces from 28.34 MPa at the first cycle to 0 MPa at the 68th cycle. The stress of element 29,296, the middle point between corner and centre, reduces to 0 MPa after the 94th cycle. The stress of the centre point reduces to 0 MPa at the 101st cycle, suggestive of the completion of the through-layer crack. From these findings, die-attachment cracks rapidly during the last 6.9% of lifecycles. The crack from corner point to 1/4 point requires 94 cycles (93.1% lifetime), and the rest crack propagates only in 7 cycles (6.9% lifetime).

5. Conclusions

In this paper, the fatigue crack evolution of Ag sintering die-attachment under power cycling loads has been investigated based on FE modelling and phase-field simulation. The thermal performance degradation for the SiC chip and the stress field distributions in the die-attachment have been analysed. The results of this research show that the power cycling induced fatigue crack propagation from the chip-side corner to the centre. Ag sintering die-attachment shows an excellent thermal conductivity, and the thermal resistance increases only after 90% of the lifetime. Fatigue crack propagation is nonlinear, which means the former 50% crack requires 93.1% of the lifetime and the latter 50% crack consumes the rest, i.e., 6.9%. The phase-field simulation shows a good agreement with the experimental results.

The major limitation of the phase-field simulation is its large computational consumptions to evaluate the crack propagation rate and predict the fatigue lifetime of the sintered Ag die-attachment. Considerably more work will need to be done to improve the phase-field model and simplify the repetitive calculation for the material fatigue.

CRediT authorship contribution statement

Yutai Su: Conceptualization, Methodology, Software, Writing - Original Draft. **Guicui Fu:** Supervision. **Changqing Liu:** Writing-Reviewing and Editing. **Canyu Liu:** Investigation, Resources. **Xu Long:** Writing- Reviewing and Editing.

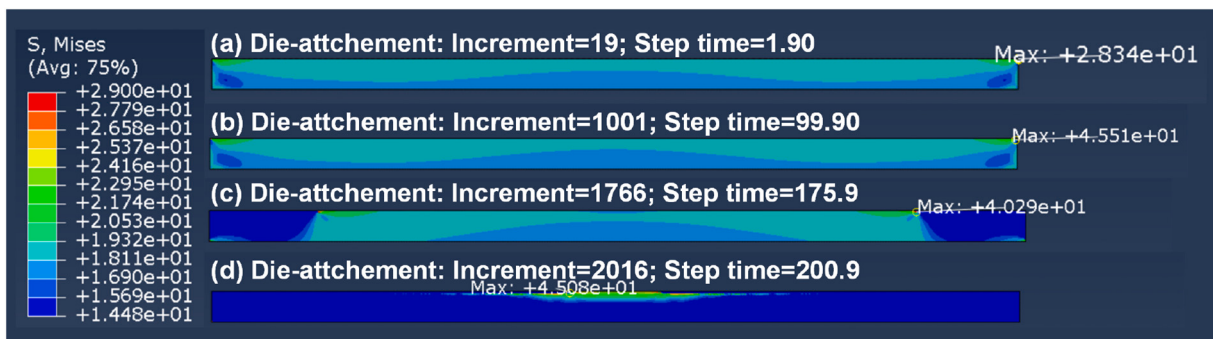


Fig. 11. Stress distributions in die-attachment during crack evolution.

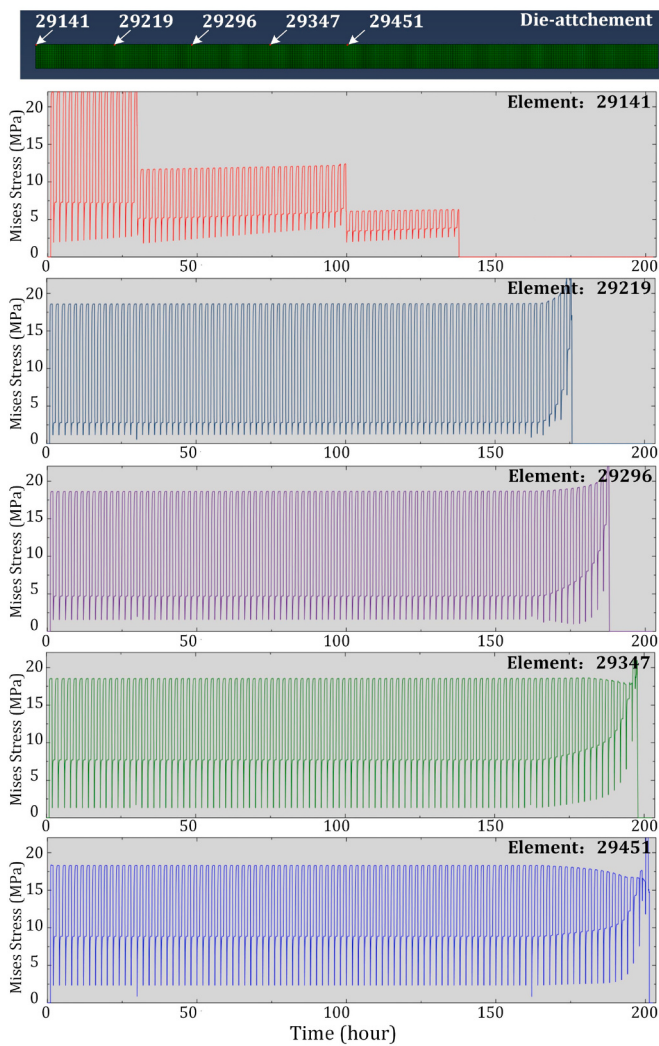


Fig. 12. Stress-time curves of the selected crack elements.

Declaration of competing interest

We declare that we do not have any commercial or associative interest that represents a conflict of interest in connection with the submitted manuscript "Fatigue crack evolution and effects analysis of Ag sintering die-attachment in SiC power devices under power cycling

based on phase-field simulation" (ESREF2021 # 149).

Acknowledgement

The authors acknowledge the funding supports provided by the China Scholarship Council (CSC) (Reference No. 201906020125), and the EPSRC research grants (UK): (i) Underpinning Power Electronics 2017 – Heterogeneous Integration (HI) project (Grant No. EP/R004501/1), and (ii) Quasi-ambient bonding to enable cost-effective high temperature Pb-free solder interconnects (QAB) project (Grant No. EP/R032203/1).

References

- [1] M.C. Lu, Enhanced sintered silver for SiC wide bandgap power electronics integrated package module, *J. Electron. Packag.* 141 (2019), <https://doi.org/10.1115/1.4042984>.
- [2] K. Sugiura, T. Iwashige, K. Tsuruta, C. Chen, S. Nagao, H. Zhang, T. Sugahara, K. Suganuma, First failure point of a SiC power module with sintered Ag die-attach on reliability tests, in: 2017: pp. 97–100. doi:10/gjgk52.
- [3] X. Long, Y. Wang, L.M. Keer, Y. Yao, Mechanical effects of isolated defects within a lead-free solder bump subjected to coupled thermal-electrical loading, *Journal of Micromechanics and Molecular Physics.* 1 (2016) 1650004.
- [4] J. Dai, J. Li, P. Agyakwa, M. Corfield, C.M. Johnson, Comparative thermal and structural characterization of sintered Nano-silver and high-Lead solder die attachments during power cycling, *IEEE Trans. Device Mater. Reliab.* 18 (2018) 256–265, 10/gjf2pm.
- [5] X. Long, Q.P. Jia, Z. Li, S.X. Wen, Reverse analysis of constitutive properties of sintered silver particles from nanoindentations, *Int. J. Solids Struct.* 191 (2020) 351–362.
- [6] X. Long, Z. Li, X. Lu, H. Guo, C. Chang, Q. Zhang, A. Zehri, W. Ke, Y. Yao, L. Ye, Mechanical behaviour of sintered silver nanoparticles reinforced by SiC microparticles, *Mater. Sci. Eng. A* 744 (2019) 406–414.
- [7] C. Miehe, F. Welschinger, M. Hofacker, Thermodynamically consistent phase-field models of fracture: variational principles and multi-field FE implementations, *Int. J. Numer. Methods Eng.* 83 (2010) 1273–1311, 10/fgnng3.
- [8] G. Molnár, A. Gravouil, 2D and 3D abaqus implementation of a robust staggered phase-field solution for modeling brittle fracture, *Finite Elem. Anal. Des.* 130 (2017) 27–38, 10/ggnqrj.
- [9] M. Dittmann, F. Aldakheel, J. Schulte, F. Schmidt, M. Krüger, P. Wriggers, C. Hesch, Phase-field modeling of porous-ductile fracture in non-linear thermo-elasto-plastic solids, *Comput. Methods Appl. Mech. Eng.* 361 (2020), 112730, 10/gf2nw.
- [10] B. Hu, J. Ortiz Gonzalez, L. Ran, H. Ren, Z. Zeng, W. Lai, B. Gao, O. Alatise, H. Lu, C. Bailey, P. Mawby, Failure and reliability analysis of a SiC power module based on stress comparison to a si device, *IEEE Trans. Device Mater. Reliab.* 17 (2017) 727–737, 10/gjgk47.
- [11] K. Sugiura, T. Iwashige, K. Tsuruta, C.T. Chen, S. Nagao, T. Funaki, K. Suganuma, Reliability evaluation of SiC power module with sintered ag die attach and stress-relaxation structure, *IEEE Trans. Compon. Pack. Manuf. Technol.* 9 (2019) 609–615, 10/gjgk49.
- [12] Y. Su, G. Fu, C. Liu, K. Zhang, L. Zhao, C. Liu, A. Liu, J. Song, Thermo-elasto-plastic phase-field modelling of mechanical behaviours of sintered nano-silver with randomly distributed micro-pores, *Comput. Methods Appl. Mech. Eng.* 378 (2021), 113729, 10/gh7zz6.